Universidade de São Paulo
Instituto de Astronomia, Geofísica e Ciências Atmosféricas
Departamento de Astronomia

Lucas Ferreira da Rosa Moda

Terrestrial Planet Formation in Protoplanetary Disks with Random Mass Depletions

São Paulo
2018

Lucas Ferreira da Rosa Moda

Terrestrial Planet Formation in Protoplanetary Disks with Random Mass Depletions

Monografia apresentada ao Departamento de Astronomia do Instituto de Astronomia, Geofísica e Ciências Atmosféricas da Universidade de São Paulo como requisito parcial para a obtenção do título de Bacharel em Astronomia.

Área de Concentração: Astronomia
Orientador: Prof. Dr. Sylvio Ferraz-Mello
Coorientador: Prof. Dr. Nader Haghighipour*

São Paulo

2018

* University of Hawaii at Manoa

to all of you that helped me, taught me, and allowed this work to be possible

Acknowledgements

First of all, to my family, who always supported me;

To my beloved Lulis, for always staying by my side even far;

To Sylvio, for being such an exemplary advisor;

To Nader, for welcoming me in Hawaii and for teaching me the ins and outs of this project (and for the awesome soccer matches);

To teachers Jane and Vera for the tips and warm support throughout all the course, but also to every professor that contributed along the way;

To all my friends, for staying together and hanging tough until this very moment;

And to all my athletes, whom I proudly teach and learn from.

Esta tese/dissertação foi escrita em LaTeX com a classe IAGTESE, para teses e dissertações do IAG.

Resumo

Esse trabalho foi conduzido na University of Hawaii (UH) at Manoa, sob a orientação do Prof. Nader Haghighipour e da coorientação do Prof. Sylvio Ferraz-Mello. O objetivo do projeto era explorar a formação de planetas semelhantes (análogos) a Marte, especialmente os cenários e condições iniciais a partir das quais um Marte verossímil foi formado.

Usamos discos protoplanetários com certos perfis de densidade e uma miríade de condições iniciais (rodamos 128 simulações no *cluster* da UH, por 2 Gyr. Todavia, apenas 64 passaram para análise final). Simulações feitas anteriormente com discos "usuais" tendiam a produzir Martes maiores e mais massivos. Para contornar esse problema, introduzimos, aleatoriamente, depleções de massa em localidades aleatórias do disco, criando inúmeros discos distintos. Conteúdo e transporte de água também foram levados em consideração.

Apesar de não termos conseguido formar um análogo de Marte, algumas conclusões interessantes puderam ser feitas a partir dos resultados: mais importante de tudo, o sistema solar interior é bastante sensível às condições iniciais; os sistemas finais produzidos por cada simulação possuem grande variedade, o que é um argumento para a hipótese de que sistemas planetários são sistemas intrinsecamente caóticos e que, por isso, devem ser encontrados nas mais diversas formas.

Abstract

This work was conducted in the University of Hawaii (UH) at Manoa, under the orientation of Prof. Nader Haghighipour and the coorientation of Prof. Sylvio Ferraz-Mello. The aim of this project was to explore the formation of planets similar (analog) to Mars, especially the scenarios and initial conditions from which a realistic Mars was formed.

We used protoplanetary disks with certain surface density profiles and a variety of initial conditions (we ran 128 of them in UH's *cluster*, for 2 Gyr. However, only 64 passed for final analysis). Previously done simulations with "regular" disks tended to produce bigger, heavier Mars. To get past this issue, we introduced random mass depletions at random locations of the disk, creating inumerous distinct disks. Water content and water delivery is taken into account as well.

Although we were not able to form a Mars analog, some interesting conclusions could be drawn from the results: most important than all, the inner Solar System is very sensible to the initial conditions; the final systems produced by each simulation have gread variety, which is an argument for the case that planetary systems are intrinsically chaotic and, therefore, should be found in the most diverse forms.

List of Figures

List of Tables

Contents

Chapter 1

Introduction

Numerous efforts to develop a coherent model for the formation of the terrestrial planets of our Solar System have been made in the past two decades. Mars, in special, has been deeply problematic. Even though dozens of sophisticated computational simulations were carried out trying to adress this problem (like Brasser (2013)), the formation of Mars remains a mystery. These simulations have had success in creating some compatible features of the inner Solar System (such as the number of planets, stable, low-eccentric orbits and Earth's water content), but tend to produce much heavier Mars-analogs. Furthermore, Mercury-analog planets are poorly understood and few studies have approached the issue; thus, its formation remains an even bigger mystery.

When we study the formation of terrestrial planets, we must take note of the orbital configuration of the giant planets, in special the mean-motion and secular resonances. Such features greatly affect the eccentricity of planetesimals and protoplanetary bodies, playing an important role on collisions, inclination variations and ejections. Haghighipour and Winter (2016) have shown that secular resonances ν_5, ν_6 and ν_{16} have strong effects on the formation of the inner planets.

Some Mars-analogs with appropriate mass have been formed when Jupiter and Saturn have initial orbits that are relatively eccentric (about 0.1; Thommes et al. (2008); Raymond et al. (2009)). Current orbits of these planets are practically circular, but early instabilities during the formation process could have led to an increase in eccentricity (Lega et al. (2013)). Damping these values to cirular orbits, however, proved to be a difficult task. Models of the origin of Earth's water suggest that a relevant amount of Earth's water was brought to its accretion zone from planetesimals and planetary embryos further than 2 AU (Morbidelli et al. (2000); O'Brien et al. (2006), Izidoro et al. (2013)); eccentric Jupiters

and Saturns, therefore, would deplete this region and cause planets formed within Earth's region to have less water content than expected. Hansen (2009) also succeeded in forming Mars (and Mercury) analogs by creating a narrow annulus of protoplanetary bodies around 1 AU.

As one might imagine, a protoplanetary disk is a turbulent and highly dinamic region - during all phases of its evolution, its physical properties are routinely changing. Inumerous processes affect these and the radial profile of the disk. Earlier simulations considered the disk to follow a power-law distribution of solid material, but, as proposed by Jin et al. (2008), regions with different viscosities can cause the material from the inner part of the disk to flow faster inward compared to the material on the outer part; this effect creates a local minimum in the disk's mass distribution in the boundary between these two regions. Izidoro et al. (2014) introduced a local minimum through *ad hoc* depletions in a specific region of the disk (around Mars location) and was able to produce some viable Mars.

Still on this topic, Raymond et al. (2005) created disks with uniform radial surface density profiles following $r^{-\alpha}$, where α varies between 0.5 and 2.5. The "standard" value for α is taken to be 1.5. They showed that steeper profiles (that is, higher values of α) produced: more terrestrial planets; faster times of formation; planets formed closer to the star; more massive planets; planets with lower water content. Haghighipour and Winter (2016) extended the work of Raymond et al. (2005), using disks with varying density profiles and adding the effects of mean-motion and secular resonances - that is, disks with different initial masses and radial profiles. Their results were also promising.

Another model was able to adress the formation of Mars (small mass and short time of formation, compared to Earth): Walsh et al. (2011) proposed the "Grand Tack" scenario, in which the giant planets migrated inward and then outward to their current orbit, depleting material during the process. However, its success is tied to a very narrow range of disk parameters, and the outward migration of giant planets has to occur very fast; the slower it is, less effective the Grand Tack model becomes. Because of this "extreme fine tuning", until now this scenario remains unlikely, and will not be explored on this work.

In sum, both Izidoro et al. (2014) and Walsh et al. (2011) were able to form Mars-analogs using the same principles (Mars forming in a mass-rich region of a disk with a non-uniform surface density profile, and then getting scattered into a local-mass-depleted region). The mechanism responsible for these non-uniformities, nevertheless, are drama-

tically distinct. While the latter uses a uniform disk surface density profile, following the classical model, and then introduces the depletion through the migration of Jupiter and Saturn, the former relies on disks that are intrinsically inomogeneous. As a result, Izidoro's model provides Mars-analogs that are purely a product of the evolution of the disk, whilst the Grand Tack model suggests that Mars is a proof of giant planets' migration. What is common to both models, however, is the dependency on the spatial distribution of the disk and the effects of the giant planets.

The present work is an improvement to the model of Izidoro et al. (2014). It already was able to produce some coherent Mars-analogs through the introduction of *ad hoc*, single local minimum. What we aim to do is introduce *random* depletions instead, running a variety of simulations with different slopes for the surface density profiles and inomogeneities that have random widths and random depletion rates at random locations. We want to see how these changes on the disk affect the planets formed.

The next section will dissect the model used, as well as give a brief introduction to terrestrial planet formation and the water delivery process. Technical details of the simulations will be discussed too.

Chapter 2

Model

2.1 Terrestrial Planet Formation

Before we dive into the model itself, it is good to have a quick overview on terrestrial planet formation. Up to this point we have already discovered more than 2000 exoplanets, and these exoplanetary systems are of astonishing variety; regardless of observational bias, we have yet to find a "common law" that governs the formation of planets for all systems. Moreover, we still have not found anything similar to our own Solar System, but, then again, observational bias plays an important role as it is much more likely to find giant planets and Super Earths - detection of terrestrial planets remains a very arduous task. Given these difficulties, it is better to first understand the process of formation of the planets of our own system. For a more complete discussion see Haghighipour (2013) and Morbidelli et al. (2012). Also, a complete flow chart can be seen on Fig. 2.1.

It all begins with a molecular cloud collapsing under its own gravity and forming a star and a disk-like structure orbiting around the central body, obeying the law of conservation of angular momentum. This circumstellar disk, made of gas and dust, is known as *nebular disk*. The growth of these dust particles to larger objects (planetesimals, planetary embryos and finally terrestrial planets) greatly depends on the mass and dynamical properties of the nebula, and happens on 4 stages:

1. Merging of dust particles through low relative velocity collisions, which results in the formation of centimeter and decimeter-sized bodies;

2. Growth of these bodies to kilometer-sized planetesimals;

3. Collision and accretion of planetesimals to form planetary embryos (Moon-to-Mars-

sized objects) in the inner Solar System, and the same process to form the cores of giant planets in the outer Solar System;

4. Accretion of gas to form the giant planets and collisional growth between planetary embryos to form terrestrial planets.

It's important to note that the physical principles behind each of these stages are significantly different, thus, it's possible to study them separately. Since rotational velocities are smaller further away from the Sun, planetesimals lying in orbits with a > 5 AU tend to collide with low relative velocities; thus, they are more likely to merge than planetesimals lying closer to the Sun. Also because of their distances, they are made mostly of ice, increasing the efficiency of sticking. Because of that, planetesimals sitting at large distances grow to few Earth-masses objects in a short time; and this process happens while the nebular gas is still present, so these objects grow and attract gas from its surroundings at the same time, forming a large body with a gaseous envelope and a mass of hundreds of Earth masses. This mechanism, known as the *core-accretion model*, is one of the main hypothesis for the formation of the gas-giant planets in the Solar System. Unlike the outer region, the accretion process for planetesimals in closer orbits is not as efficient (and their composition is more rocky), causing the formation of terrestrial bodies to take several hundred million years.

Another model for the formation of such planets has been proposed: the *disk-instability model* (Boss (2003)). It consists of local gravitational instabilities in the solar nebula, which fragments the disk into massive clumps that contract and form gas-giant planets in short times. The major issue with this model is that it lacks an efficient cooling process, needed to quickly take away the energy from the clumps before it disperses.

Now let's take a closer look at each step of the process of terrestrial planet formation.

2.1.1 From Nebula to Planetesimals

At first, micrometer-sized dust particles (mainly on a Brownian motion) collide with one another with very low relative velocities. Because of this "gentle" collisions, van der Waals forces act between their surfaces and the grains stick to one another, resulting in a fractal growth to larger aggregates.

Whereas the "first phase" of terrestrial planet formation is well understood, the growth of larger aggregates to kilometer-sized planetesimals is quite problematic. As size increases, the coupling of dust particles to the gas weakens, so their relative velocities increase as well. In fact, centimeter-sized objects' sticking efficiency is tremendously worse, and their relative velocities become so large that their collisions, rather than resulting in merging, cause either bouncing or fragmentation (known as *bouncing* and *fragmentation barriers*). Adding to the issue, other factors, such as the sub-Keplerian rotational velocities of the gas molecules, which results in the transfer of angular momentum from solid bodies to the gas and the consequent "drift" of these bodies toward the star, contribute to make the scenario even more complicate. This radial drift, whose time of approach is proportional to the size of the body, increases the relative velocities and makes it even more probable that collisions result in fragmentation; the sticking properties of solid materials also dwindle with size. Since meter-sized objects have the fastest radial drifts, this process is known as *meter-size barrier*. It implies that, even if the bouncing and fragmentation barriers are somehow overcome, impact velocities of meter-sized objects are so high that it becomes very unlikely that they will merge; the smaller resulting fragments would then undergo the same process and the cycle would repeat until all material drifts toward the star and there is nothing avaliable for the formation of planetesimals.

Still, planets and many kilometer-sized bodies are out there. This means that there is another mechanism (or mechanisms) capable of surpassing the difficulties imposed by the centimer-sized and kilometer-sized barriers; we just don't know yet.

2.1.2 From Planetesimals to Planetary Embryos (Runaway and Oligarchic Growth)

This phase begins when enough planetesimals are formed and the dynamics of accretion becomes dominated by the effect of the gravitational attraction between them. During this phase, big bodies grow faster than small ones and their relative mass difference rapidly increase - this process is known as *runaway growth*. This rate is an increasing function of the body's mass, thus, runaway growth comes to a halt when the masses of the large bodies become too dominant and begin to dictate the dynamics. For mathematical proof see Morbidelli et al. (2012). Runaway growth forms closely packed together Moon-to-Mars sized objects at 1 AU on timescales of around 10^5 to 10^6 years. Another interesting feature of the runaway growth is that because it is a *local* process, the embryos formed should

have little radial mixing and similar chemical compositon.

Now, relative velocities between small bodies once again increase and their collisions become disruptive. Hence, planetesimals only participate in the growth of embryos - this process is known as *oligarchic growth*.

The embryos formed are not yet terrestrial planets, since they are too numerous, too close to one another, not massive enough and don't contemplate the tens-to-hundreds of millon years timescale necessary to form a terrestrial planet.

2.1.3 From Planetary Embryos to Terrestrial Planets

The still present nebular gas tends to stabilize the orbits of the remanining embryos, continuoulsy damping their eccentricities to circular orbits. For bodies in the asteroid belt region, however, Jupiter resonances prevent this damping effect and embryo collisions are not so gentle; furthermore, many objects of this regions are highly excited and get ejected toward a collision with the Sun or an ejection of the Solar System on a hyperbolic orbit. Some of them are scattered to an inner region, where they are accreted by stable embryos.

The typical final product (as many N-body integrations demonstrated) is an asteroid belt devoid of embryos and populated by a few planetesimals on stable orbits and a few terrestrial planets on stable orbits formed between 0.5 and 2 AU at timescales of tens of millions of years. All in all, in spite of the great computational resources needed and the number of bodies limitation (a few thousands, much less than the real protoplanetary disk had), many of our Solar System's features can be reproduced with surprising accuracy.

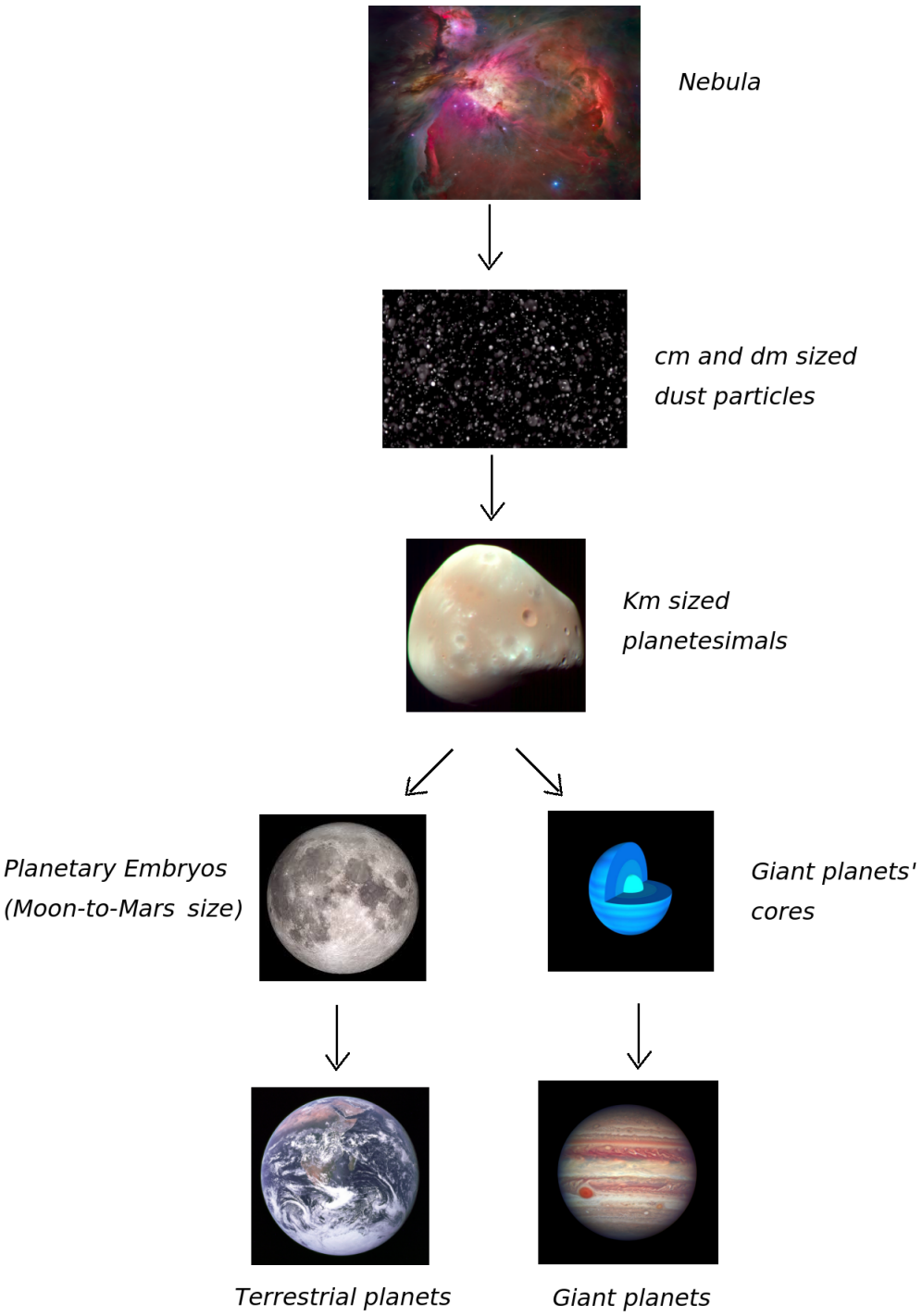

Figure 2.1: Flow chart of planet formation. Figures, from top to bottom: Orion Nebula, dust particles, Deimos (smaller of the moons of Mars), Moon, schematic of Jupiter's core, Earth, and Jupiter.

2.2 Protoplanetary Disk

Following Kokubo and Ida (1998); Kokubo and Ida (2000), we considered a disk in which runaway and oligarchic growth already took place and resulted in a bi-modal distribution of the mass. Since we are interested on the late stage of terrestrial planet formation, we considered a disk extending from 0.5 AU to 4.5 AU, populated by planetesimals and planetary embryos, with half of its mass coming from each population. According to O'Brien et al. (2006) and Morishima et al. (2008), the presence of planetesimals provides the needed dynamical friction to damp the eccentricities and inclinations of the embryos. Planetesimals only interact with planetary embryos and the giant planets (in other words, they don't interact between themselves), and have masses between 0.001 and 0.008 Earth Masses.

The masses of the planetary embryos scale as (Kokubo and Ida (2000); Raymond et al. (2005), Raymond et al. (2009)):

$M \sim r^{3(2-\alpha)/2}\Delta^{3/2}$

Where α is the slope of the surface density profile and Δ is the number of mutual Hill radii (the Hill radii is the radius of the Hill sphere, which defines the region in which a body becomes gravitationally tied to the attractor). We consider the embryo-to-planetesimal mass-ratio to be ~ 8 at 1.5 AU (Raymond et al. (2009)), and the surface density of the disk to have radial profiles with three different slopes: 1.5, 1 and 0.5.

Next we added depletions through a parameter β, the depletion rate ($0 < \beta \leq 1$), that represents the percentage of the mass that has been locally taken away. Izidoro et al. (2014) considered just one depletion region, placed either from 1.1 AU to 2.1 AU or 1.3 AU to 2.0 AU, with depletion rates of 25%, 50% or 75% (Fig. 2.2). Our model follows basically the same structure as Izidoro's, but differs in the sense that, rather than plucking just one "gap" in the disk, we generate:

- random number of gaps;
- with random widths;
- at random locations;
- with random depletion rates β.

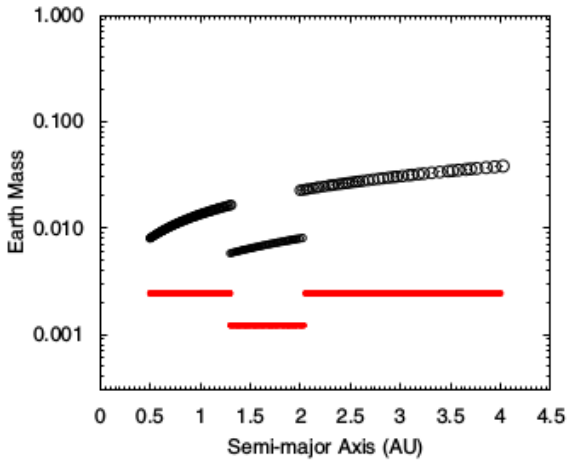

Figure 2.2: One of the disks used by Izidoro et al. (2014). Notice the local mass depletion between 1.3 AU and 2.0 AU. Planetesimals are all considered to have the same mass - 0.0025 Earth masses. Figure taken from Izidoro et al. (2014).

Adding all together, the disk surface density profile is given by:

$$\Sigma(r) = \begin{cases} \Sigma_1 (r/1AU)^{-\alpha}; \text{ outside depleted regions} \\ (1-\beta)\Sigma_1 (r/1AU)^{-\alpha}; \text{ inside depleted regions} \end{cases}$$

Where $\Sigma_1 = 8\text{g cm}^{-2}$, $\alpha = 1.5$, 1 or 0.5 and β is the randomly generated depletion rate for each gap. Figs. 2.3 and 2.4 illustrate these depletions.

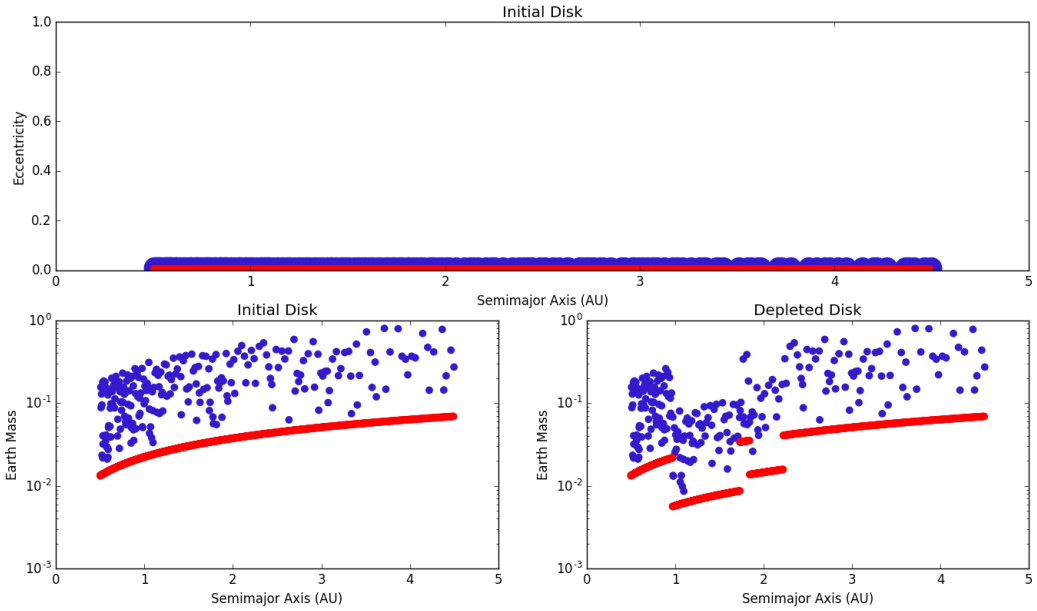

Figure 2.3: Disk visualization of one of our simulations. Planetary embryos are shown in blue and planetesimals in red. Top panel shows initial disk - all bodies have very low eccentricities. Bottom panels show the masses in Earth masses before (left) and after depletions (right). Notice the gaps in the bottom right figure.

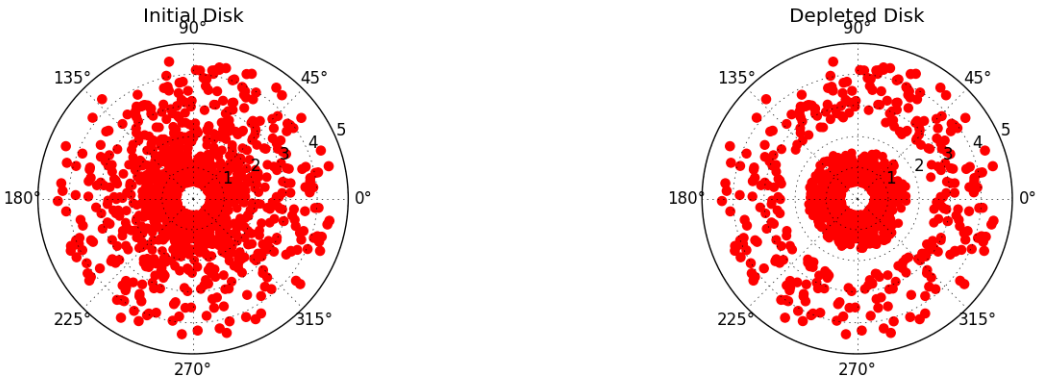

Figure 2.4: Top view from one of the disks. Notice that depletions are *not* spatial; that is, bodies inside depleted regions stay where they were, but are less massive. The figure shows a case when $\beta = 1$; only in that case there is spatial depletion, as noticed by the lack of bodies on the right figure near the second circular dotted line (between 1 AU and 2 AU). For all other values of β the bodies inside depletion regions of the right figure would be represented by smaller circles, since their masses have been depleted.

We assume that at the beginning of our simulations Jupiter and Saturn are fully formed and are at their current orbits; the gas disk has already fully dissipated and secular resonances' effects are also considered. Planetary embryos were spaced from one another

at distances of 3-6 mutual Hill radii (Kokubo and Ida (2000)). The orbital inclinations for all bodies were randomly generated and are no bigger than 10^{-3} deg; mean anomalies were taken randomly from 0° to 360° and the arguments of periastron and longitudes of ascending nodes set to zero. Both planetesimals and planetary embryos are initially in circular orbits.

The simulations consisted of 130-650 planetary embryos and 1520 planetesimals and were carried out using the hybrid integrator of the N-body integration package MERCURY (Chambers (1999)), during 2 Gyr with a timestep of six days. Although this is a greater time than the timescale of terrestrial planets formation, it's good exercise to extend the simulations for further times to have certainty of the stability of the system.

In our simulations we considered complete merging; that is, perfectly inelastic collisions - every time embryos collide, they merge. Simulations using Smooth Particle Hydrodynamics (SPH) show that complete merging is rare - rather, they just "hit and run" or produce fragments. Kokubo and Genda (2010) approached elastic collisions and fragmentation using SPH simulations and found out that the final product is barely affected by those type of collisons. And, because execution time grows substantially (as each new fragment becomes a new body), including elastic collisions is completely expendable and unrelatable to the final result. What happens is that, even if objects fragment during collisions, the bodies stay in the system (as well as the total mass is conserved) and these new particles will eventually be accreted. Therefore, including those "imperfections" only delays what is already achievable with perfect merging and requires more time of execution, rendering useless.

2.3 Water Delivery

The origin of Earth's and the inner planets' water is a subject of intense debate. The chemical composition of the nebula was greatly affected by its temperature gradient (hotter and denser toward the center). As a result, close to the center only metal and silicates condensed, while more volatile materials condensed at longer distances. Beyond the so called snow-line, water condensed in large quantities to form ice-based bodies, the comets.

As Haghighipour (2013) noted, Earth has little amount of water: about 0.02 % of its mass is contained in its oceans, and about 10 times of the oceans' mass contained inside

Earth's mantle in the form of internal water. All in all, this points to Earth having a WMF (water mass fraction) of about 0.2%, still much higher than expected from a body at 1 AU (Fig. 2.5).

Three main sources for this water content have been proposed. The first comes from a nebular origin: Earth gravitationally captured a hydrogen-rich atmosphere of nebular gas and oxidized it to form water. The second is that Earth's water came from the bombardment of comets coming from the Main Belt. And finally the third suggests that Earth accreted water from planetesimals and/or planetary embryos originally formed on the outer asteroid belt and scattered inward (by the effects of the secular resonances of Jupiter and Saturn). Each of the hypothesis have its own problems; it is very likely that the water delivery process can not be explained by one of those theories alone, but rather as a combination of them. For more detailed discussion on this topic, see Haghighipour (2013) and Morbidelli et al. (2012).

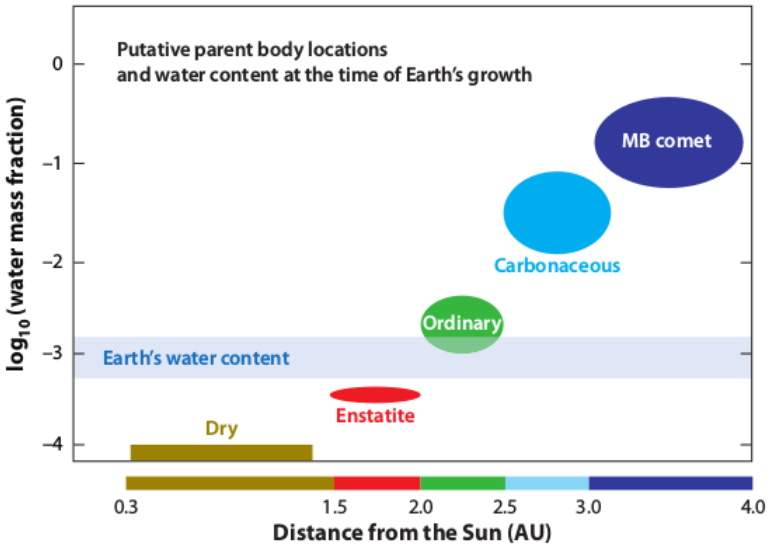

Figure 2.5: Water content based on distance and parent bodies. Main Belt Comets are essentialy made of water and sit at distances > 3 AU, while carbonaceous chondrites (including C-type asteroids) have 5-10% of their mass in the form of water and lie in the asteroid belt. Ordinary chondrites (S-type asteroids) are predominant between 2 AU and 2.5 AU and are believed to have only about 0.1% of their mass in the form of water. Enstatite chondrites (E-type asteroids) are very dry and contain about 0.01% of their total mass in the form of water. Finally, bodies inside 1.5 AU are essentialy dry. Figure taken from Morbidelli et al. (2012).

For our simulations, we considered bodies closer to 2 AU to be dry (WMF $= 0$), bodies between 2 and 2.5 AU to have 0.001 WMF (0.1%) and bodies further out to have 0.05 WMF (5%). Tracking the water delivery was possible due to a file that contained information

about collisions (Fig. 2.6). Adopted color code was:

- WMF $< 0.00001 \rightarrow$ Red;
- WMF in [0.00001, 0.0001] $\rightarrow$ Light Red;
- WMF in [0.0001, 0.001] $\rightarrow$ Orange;
- WMF in [0.001, 0.01] $\rightarrow$ Yellow;
- WMF in [0.01, 0.02] $\rightarrow$ Light Green;
- WMF in [0.02, 0.03] $\rightarrow$ Green;
- WMF in [0.03, 0.05] $\rightarrow$ Light Blue;
- WMF $> 0.05 \rightarrow$ Blue;

```
805 EM53     was hit by P369     at     2279756.797 years
806 EM45     was hit by P475     at     2296852.142 years
807 EM185    ejected at    2308890.3490760 years
808 EM20     was hit by P330     at     2323567.855 years
809 EM89     was hit by P67      at     2326761.392 years
810 EM184    was hit by P1304    at     2386286.540 years
811 EM53     was hit by P681     at     2400115.047 years
812 EM45     was hit by P357     at     2403140.967 years
813 EM127    was hit by P401     at     2406985.718 years
814 EM19     was hit by P677     at     2407852.148 years
815 P1406    ejected at    2414728.5420945 years
816 EM187    was hit by P963     at     2428120.455 years
817 P1085    ejected at    2436111.7043121 years
818 EM11     was hit by P32      at     2470977.386 years
819 EM53     was hit by P332     at     2483801.383 years
820 P1216    ejected at    2483835.7289528 years
821 EM11     was hit by P434     at     2493776.229 years
822 EM11     was hit by P292     at     2502683.499 years
823 EM11     was hit by P546     at     2513631.937 years
824 P988     collided with the central body at    2515513.7742323 years
825 EM170    was hit by P1224    at     2515717.796 years
826 P1508    ejected at    2521524.4353183 years
827 EM208    was hit by P1242    at     2522570.367 years
828 EM190    was hit by P1231    at     2530649.537 years
```

Figure 2.6: Part of the tracking file for one of the simulations. It shows which bodies collided (in case of planetesimals they simple merge with the embryos. For embryo-embryo collisions we first need to check whose mass is bigger. Remember that planetesimal-planetesimal collisions do not ocurr), were ejected or collided with the Sun. Adding the masses, excluding bodies ejected or integrated to a bigger object and calculating the new WMF for each line of the file makes sure the final bodies have the correct WMF.

2.4 Simulations

We ran a total of 128 simulations, using three different slopes for the surface density profile: $r^{-1.5}$, r^{-1} and $r^{-0.5}$. They were given nicknames based on the slope: "Main"

(because 1.5 is the slope of the standard model), "One" and "Half", respectively. Then we built uniform protoplanetary disks (without depletions): 8 distinct configurations for Main (this was achieved by slightly varying the minimum and maximum values for the mass at 1 AU) and 4 distinct configurations for both One and Half. Finally, each of the disks was depleted in 8 different ways, with the conditions (and numeration) as follows:

- 1: maximum of 8 gaps, widths in [0.3, 0.8] and β in [0.2, 0.8];
- 2: maximum of 8 gaps, widths in [0.3, 0.8] and β in [0.1, 0.5];
- 3: maximum of 6 gaps, widths in [0.2, 0.7] and β in [0.2, 0.8];
- 4: maximum of 6 gaps, widths in [0.2, 0.7] and β in [0.1, 0.5];
- 5: maximum of 5 gaps, widths in [0.5, 0.8] and β in [0.2, 0.8];
- 6: maximum of 5 gaps, widths in [0.5, 0.8] and β in [0.1, 0.5];
- 7: maximum of 12 gaps, widths in [0.1, 0.4] and β in [0.1, 0.4];
- 8: maximum of 12 gaps, widths in [0.1, 0.4] and β in [0.2, 0.8].

This means we have 8 types of depletion:

- intermediate number of gaps, large widths and big depletions;
- intermediate number of gaps, large widths and small depletions;
- few gaps, intermediate widths and big depletions;
- few gaps, intermediate widths and big depletions;
- few gaps, large widths and big depletions;
- few gaps, large widths and small depletions;
- lots of gaps, narrow widths and small depletions;
- lots of gaps, narrow widhts and big depletions.

Not all combinations were explored. Choices were made based on computational resources available and physical relevance: for example, lots of gaps with large widths would lead to too many depletion - the disks would become somewhat empty, and the bodies would be too light. Conversely, few gaps with narrow widths would lead to very little depletion, and the disks would resemble the classical ones (like Mayer et al. (2002)). Further simulations may prove this wrong, but since we had to make choices, the aforementioned types of depletions were considered more promising. See example on Fig. 2.7.

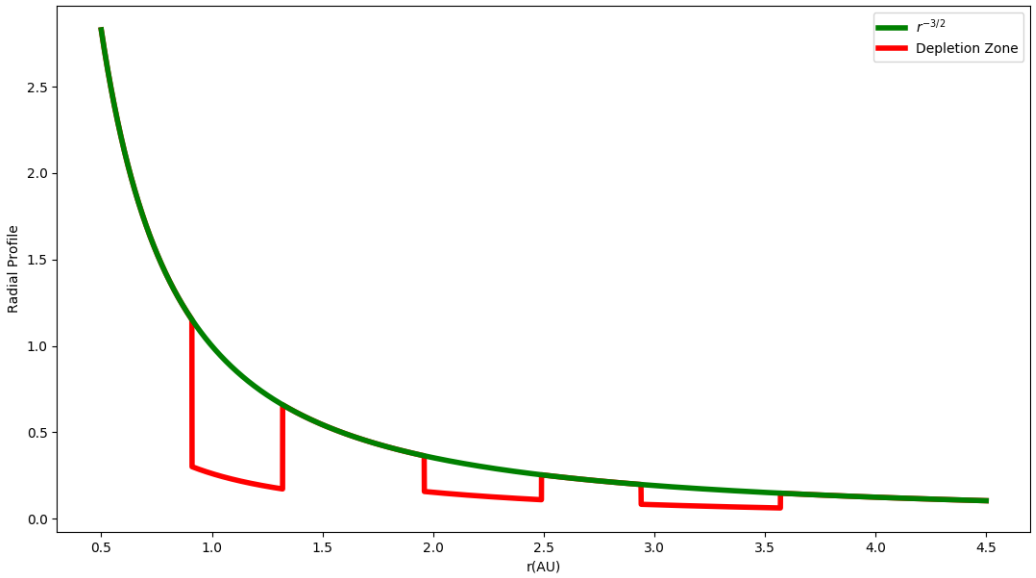

Figure 2.7: Example of how the depletions look like. In the Surface Density Profile x Radial Distance space, we can see in green how the density profile function looks like for a "clean" disk ($r^{-3/2}$). In red are the depletion zones, where the density function is scaled by a factor of $1 - \beta_n$: this leads to a step function.

Simulations were named with a letter representing the slope ("m", "o" or "h"), followed by "emb", a number between 1 and 8 representing the configuration of the disk, "g", and another number between 1 and 8 representing the depletion configuration used. For example, "memb3g6" is the simulation using 1.5 as the slope of the profile distribution, the third configuration of the disk and the sixth configuration for depletions.

Summarizing, we have:

- 8 configurations for $r^{-1.5}$ with 8 different depletion configurations for each = 64 simulations;

- 4 configurations for r^{-1} with 8 different depletion configurations for each = 32 simulations;
- 4 configurations for $r^{-0.5}$ with 8 different depletion configurations for each = 32 simulations.

Totaling 128 simulations. Since depletions are randomly generated, an output file with the configurations used was created for each simulation, as shown by Fig. 2.8:

```
Number of Embryos = 293
Number of Gaps = 4
Minimum and Maximum width of gaps = 0.2 and 0.7
Minimum and Maximum depletion rates = 0.2 and 0.8
1.55 AU has depleted material (38.7 % of the disk)

Gap number 1 has a width of 0.46 AU, starting at 0.72 AU and ending at 1.18 AU with a depletion rate of 43.43 %
Gap number 2 has a width of 0.64 AU, starting at 1.36 AU and ending at 2.00 AU with a depletion rate of 74.06 %
Gap number 3 has a width of 0.20 AU, starting at 2.15 AU and ending at 2.35 AU with a depletion rate of 54.59 %
Gap number 4 has a width of 0.24 AU, starting at 2.36 AU and ending at 2.60 AU with a depletion rate of 35.82 %
```

Figure 2.8: One of the output files. It gives the number of embryos in the simulation, number of gaps, maximum and minimum widths and depletion rates of those, as well as the percentage of the disk that has depleted material and information for each gap (width, starting and ending location and depletion rate). Since our model is stochastic by nature, there was no need to restrain gap overlaping and thus it was allowed.

Unfortunately, half of our simulations became unusable due to problems related to the cluster. Our 64 "healthy" simulations are (all g included): memb1, memb2, memb4, memb5, memb6, memb8, hemb2, oemb3. At least the majority of the main slope simulations were intact, but more need to be done in the future.

Chapter 3

Results

3.1 General Properties

A total of 330 planets were formed on 64 simulations, an average of 5.15 planets per simulation (Fig. 3.1). Most of them produced 3 to 7 planets, although one produced 2 and another one produced 11 planets.

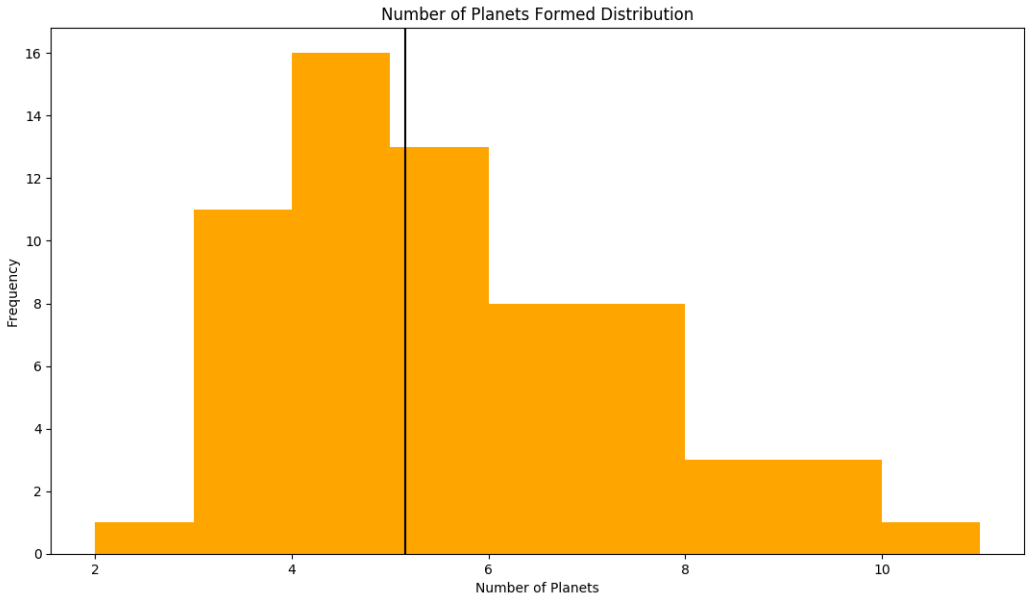

Figure 3.1: Histogram of the number of planets formed by the 64 simulations. The black vertical line shows the average number of planets formed (5.15).

Of all our simulations, *none* produced a Mars analog - we consider a Mars analog to be: between 1.4 AU and 1.6 AU (10% margin), and to have between 5% and 15% of Earth's Mass. However, 16 *Mars-like* planets were formed (we consider "like" planets to be within their actual location range of 10%, regardless of mass); of those 16, eight were more massive

than Earth, and eight were less massive than Earth. Two cases stand out: In hemb2g5 the Mars-like planet is at 1.49 AU and has 0.5 M_{Earth}, and is also dry. However, its orbit is extremely eccentric (0.462). Our "best result" for Mars came in memb2g8, where a 0.04 M_{Earth} planet at 1.59 AU was formed. However, its orbit is also eccentric (0.135) and it is very wet (WMF of 0.05); also, it is surrounded by two other planets at 1.35 AU and 1.73 AU.

For Earths the scenario is better: *two* simulations produced Earth analogs: memb1g7 produced a planet at 0.99 AU with 0.99 M_{Earth}, and memb6g8 produced a planet at 0.99 AU with 0.93 M_{Earth}. Both planets have low eccentricities (< 0.1) and are three to six times drier than our planet. Considering Earth-like planets, we had 18 cases, of which 15 were more massive than Earth (Super Earths). The mass distribution of the planets formed are shown on Fig. 3.2 and the percentages of planets formed based on mass range are on Tab. 3.1.

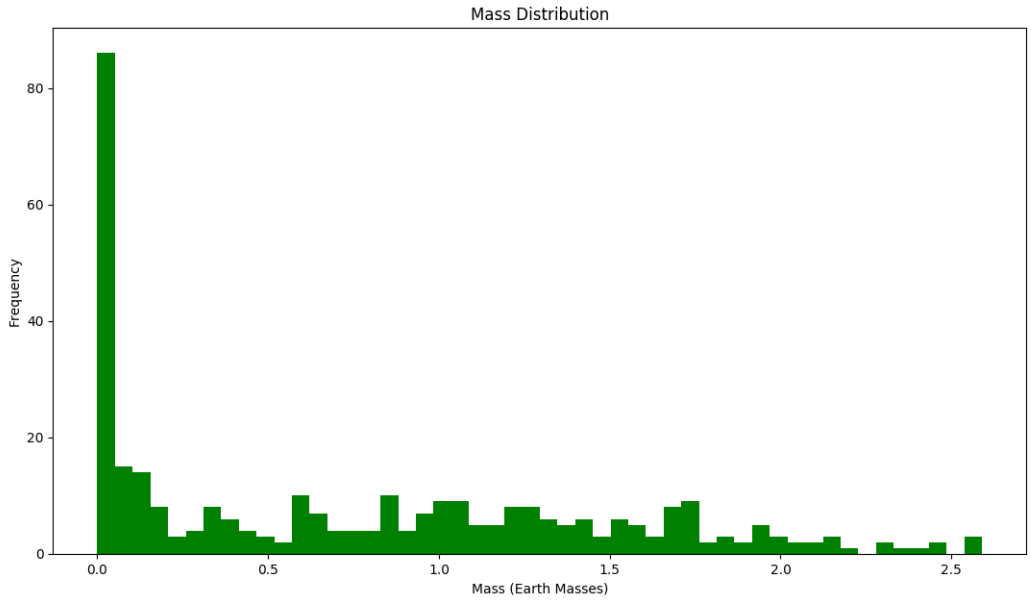

Figure 3.2: Histogram of the mass of all the planets formed by the 64 simulations.

Table 3.1 - Percentage of planets formed based on mass range. The Group column indicates the discriminant used to select the ranges.

Mass (Earth Masses)	Percentage	Group
< 0.5	26%	Mercury, Ceres
0.05-0.15	8%	Mars
0.15-0.7	18%	Not Expected
0.7-0.9	6%	Venus
0.9-1.1	8%	Earth
>1.1	32%	Super Earth

The vast majority of our planets had small masses (less than 20% of Earth's mass); almost all of them are present in the asteroid belt or near 2 AU, representing big bodies in the region (like Ceres). Those closer than 2 AU might have been accreted by bigger, nearby planets if simulations were integrated for a longer period. Or (why not?) they could represent terrestrial planet's moon prototypes, as many of them are close to a bigger planet. Other than that the distribution is relatively balanced between 0.5 M_{Earth} and 2 M_{Earth}; massive planets (> two times the Earth's mass) are relatively rare. Interestingly enough, more than half (58%) of the planets are either too massive (Super Earths) or too light (Asteroids, lighter than Mercury). Also relevant is that 18% of the planets have masses that are not present in any terrestrial body of our Solar System (more massive than Mars, but less massive than Venus); all three terrestrial planets (Venus, Earth and Mars) have similar chances of formation: 6%, 8% and 8%, respectively. If we make a raw estimation and take the chance to form a "perfect" inner Solar System (Venus, Earth and Mars analogs) to be just the multiplication of the odds of each planet's formation, we have:

$$P(perfect) = P(Venus) * P(Earth) * P(Mars) = 0.06 * 0.08 * 0.08 = 0.000384$$

This means that, for each simulation, the probability that it will reproduce a perfect inner Solar System is about 0.04%! On average, one on every 1600 simulations will yield such a system. If we took about 3 months to run 128 simulations, it would take approximately one and a half year of processing to get a perfect system.

The semi-major axis distribution and percentage of planets formed based on semi-major axis range are shown below on Fig. 3.3 and Tab. 3.2:

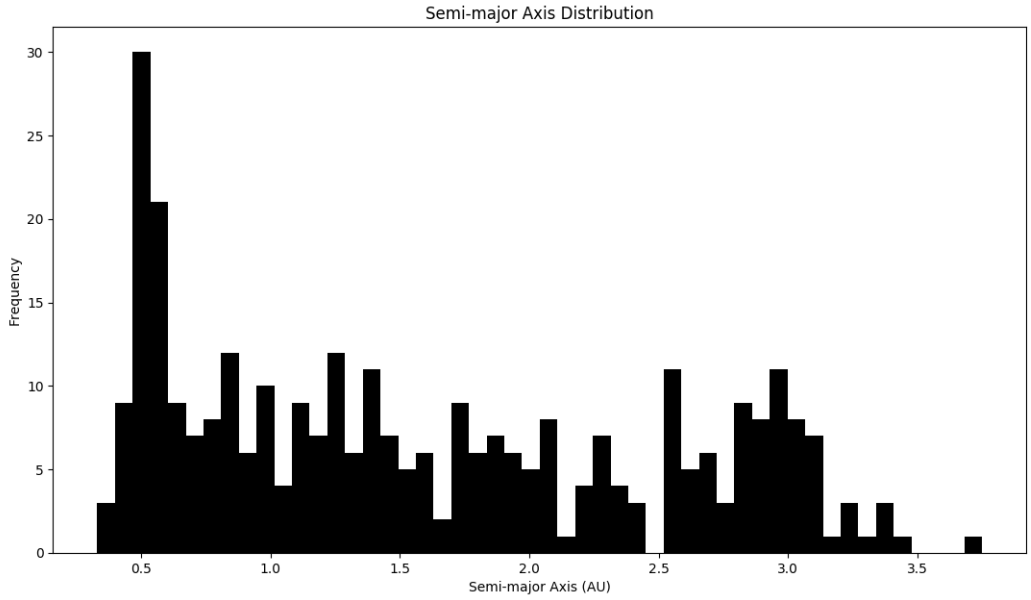

Figure 3.3: Histogram of the semi-major axis of all the planets formed by the 64 simulations.

Table 3.2 - Percentage of planets formed based on semi-major axis range. The Group column indicates the discriminant used to select the ranges.

Semi-major axis	Percentage	Group
< 0.9	31%	Inner than Earth
0.9-1.1	6%	Earth
1.1-1.4	12%	Between Earth and Mars
1.4-1.6	6%	Mars
1.6-2.5	19%	Expected Gap
> 2.5	26%	Asteroid Belt

The majority of our planets were formed inside 1 AU (especially close to 0.5 AU). Then again, this region is poorly understood and was not the main focus of this project. There are two distributions: between 0.8 AU and 1.6 AU (representing the region of Venus-Earth-Mars) and another one between 2.5 AU and 3 AU (where Ceres is located). However, we expected a "gap" between those two regions, but we see that many planets (19%) were formed around 2 AU. What might be happening is that, because of local depletions, embryos that grow in those areas are not massive enough to throw others out. That results in embryos staying and growing to larger sizes. Again, Mars and Earth share a similar property (6% of chance of formation for both), as for the case of the mass. For

a zoom on the Earth/Mars analog region (0.9 AU to 1.6 AU) see Fig. A.1 in A.

The water mass fraction distribution and percentage of planets formed based on water mass fraction range are shown below on Fig. 3.4 and Tab. 3.3:

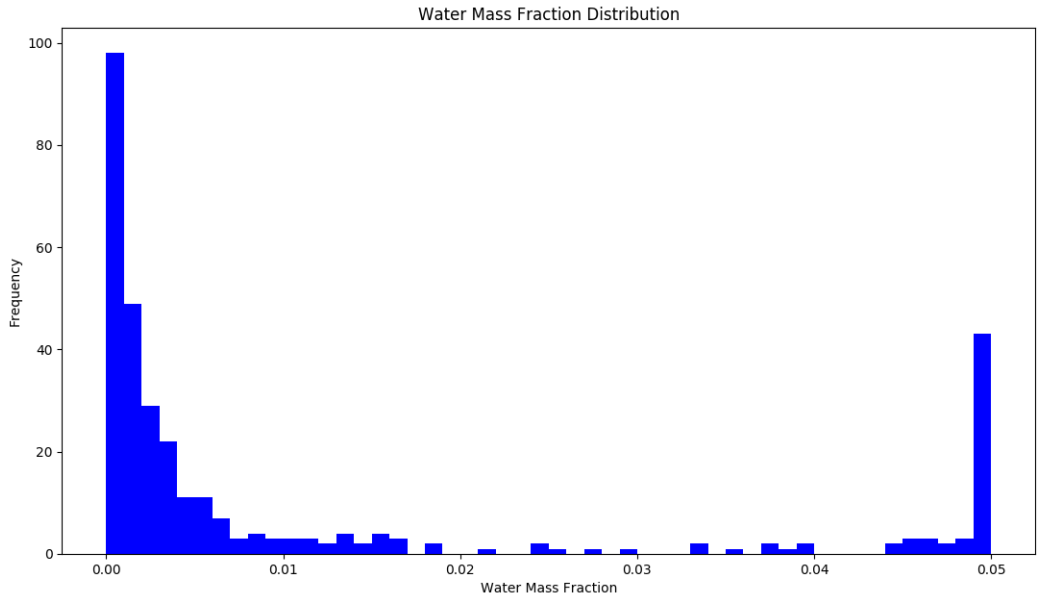

Figure 3.4: Histogram of the water mass fraction of all the planets formed by the 64 simulations.

Table 3.3 - Percentage of planets formed based on water mass fraction range. The Group column indicates the discriminant used to select the ranges.

Water Mass Fraction	Percentage	Group
< 0.001	33%	Dry
0.001-0.003	20%	Earth
0.003-0.03	27%	Wet Planets
0.03-0.05	7%	Disturbed Asteroids
0.05	%13	Untouched Asteroids

We can see a bimodal distribution of the water mass fraction of the planets formed. Most of them are extremely dry (< 0.001, 33%), which makes sense, since the inner Solar System is mostly dry. Another peak is observed at WMF = 0.05 (13%), which represents the wet bodies of the asteroid belt that were "untouched" throughout the evolution of the system (remember that the initial WMF of bodies further than 2.5 AU was set to 0.05). The remaining, less numerous planets are either wet asteroids that interacted with drier embryos coming from the inner Solar System (those with WMF > 0.03) or terrestrial

embryos that accreted wet bodies scattered inside by the effects of secular resonances. For a zoom on the "Earth WMF" region (0.001 to 0.003) see Fig. A.2 in A.

The eccentricity distribution and percentage of planets formed based on eccentricity range are shown below on Fig. 3.5 and Tab. 3.4:

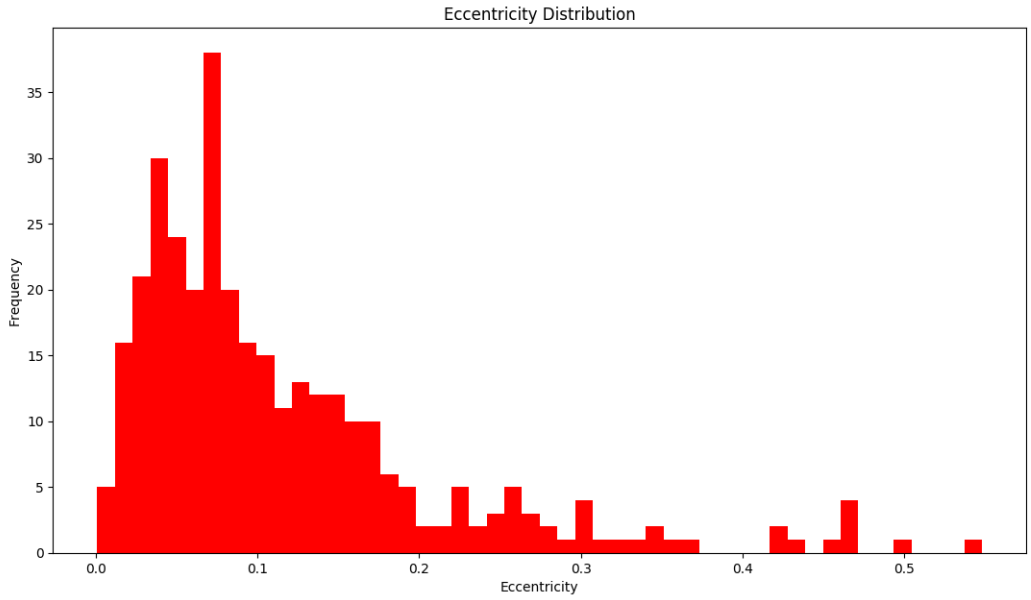

Figure 3.5: Histogram of the eccentricity of all the planets formed by the 64 simulations.

Table 3.4 - Percentage of planets formed based on eccentricity range. The Group column indicates the discriminant used to select the ranges.

Eccentricity	Percentage	Group
< 0.1	58%	Circular
0.1-0.2	28%	Intermediate
> 0.2	14%	Eccentric

Most of the planets formed (86%) have low (< 0.1) or intermediate eccentricities (up to 0.2), which is expected. Eccentricity has a negative correlation, indicating that eccentric bodies are rarer (maybe they passed on the "edge" of the resonance's areas); in every simulation many bodies were quickly ejected of the system.

3.2 Classification Based on Type of Depletion

We can divide the depletions in three types: "Few" (_emb3, _emb4, _emb5 and _emb6), "Intermediate" (_emb1 and _emb2) and "Lots" (_emb7, _emb8). Making the same comparison with those groups:

- Few: Percentages for water mass fraction and eccentricity are similar to general results. Planets formed more frequently in the Asteroid Belt (29% against 26%) and less frequently on both Mars and Earth regions (a drop of 1%). As for the mass, both Venus and Mars groups got a 2% raise, while the Earth group saw a 3% drop. 7 Earth-like planets derived from these simulations (all more massive than Earth), as well as 7 Mars-like planets, of which 5 are less massive than Earth. See example on Fig. 3.6;

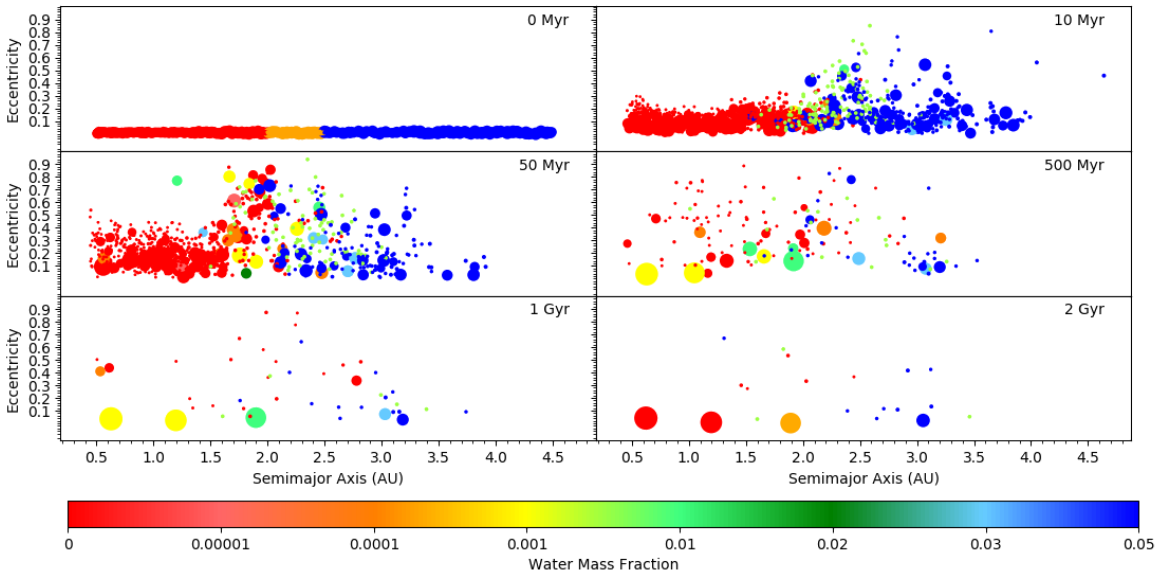

Figure 3.6: Snapshots for the eccentricities as a function of semi-major axis of memb5g6. The final product is on the bottom right panel and the time of the snapchot is on the upper right corner of each panel. Note that all bodies initially have circular orbits, then planetesimals (small circles) become highly excitated by secular resonances, and final embryos have low eccentricities, as expected. Bodies are scaled according to the cubic root of their masses ($M^{1/3}$). Color coding represents the water-mass fraction of the body.

- Intermediate: Percentages for semi-major axis and eccentricity are similar to general results. Planets tended to be a little drier, though, as the "Untouched Asteroids"

group represent 4% with this depletion type rather than 7% on the general results. Also, for the mass, Mars, Venus and Not Expected groups are slightly less frequent, whereas Earth group planets are almost twice as present as in the general results (15% against 8%); 5 Earth-like planets derived from these simulations (all more massive than Earth), as well as 4 Mars-like planets, also all more massive than Earth;

- Lots: Percentages for mass, water mass fraction and eccentricity are similar to general results. However, analyzing the semi-major axis, less planets are formed in the asteroid belt (21%, against 26%) and more are formed in both Mars and Earth regions (both 7.5% against 6%, an upgrade of 1.5%). 6 Earth-like planets derived from these simulations (3 of which were less massive than Earth), as well as 5 Mars-like planets (2 less massive than Earth, 3 more massive). The only two Earth analogs also came from this depletion type, as well as the "closest" Mars analog. See example on Fig 3.7.

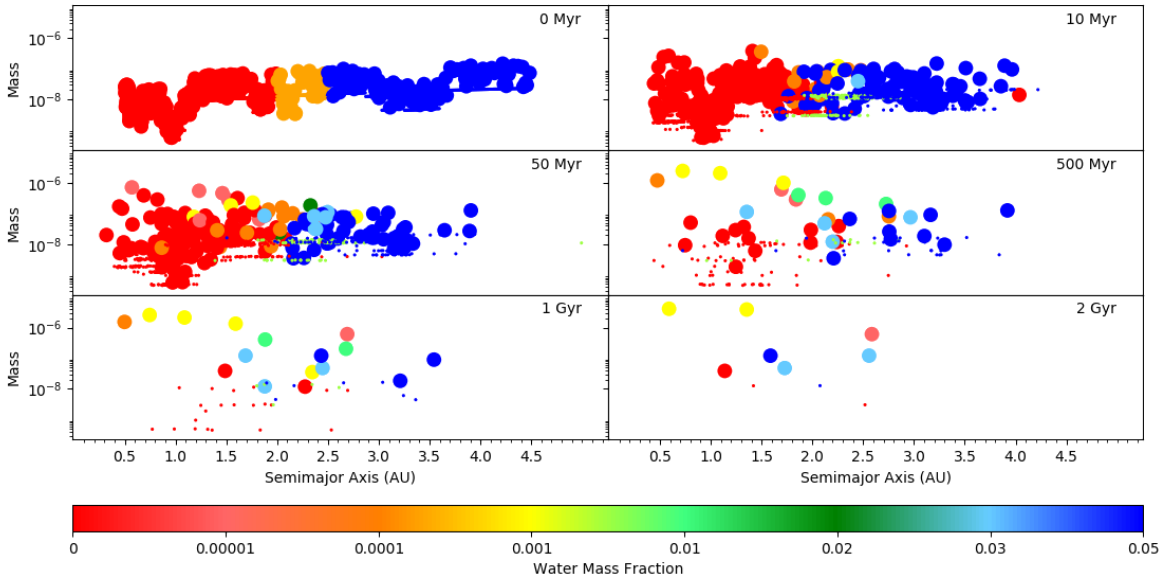

Figure 3.7: Snapshots for the masses as a function of semi-major axis of memb2g8. Big circles represent embryos and small circles represent planetesimals. The final product is on the bottom right panel and the time of the snapchot is on the upper right corner of each panel. Note the depletions on the first panel and the water delivery process happening through time. Color coding represents the water-mass fraction of the body. This is a case of the "lots" type, and near 1.6 AU (in dark blue) there is our closest Mars analog, surrounded by two other planets nearby (in light blue and yellow).

For all depletion types the average number of planets formed is close to 5 (5.0, 5.125 and

5.0, respectively). This indicates that depletion type *does not* play a role in the number of planets formed. The histograms for each depletion type are similar to the histograms considering all simulations.

In short, the type of depletion changes the properties of the final ensemble, even though more simulations are needed to strengthen the differences. The most interesting result derived from this analysis is that the "lots" type shows some promise: it is the depletion type in which most planets formed on Mars and Earth region (and less on the Asteroid Belt, meaning that embryos further than 2 AU were more efficiently scattered inwards. Conversely, the "few" type has the exact opposite property) and also the only type that produced Earth analogs, as well as the closest Mars analog. The only 3 Earth-like planets that are less massive than Earth were formed on these systems as well. Apparently, this indicates that our disk is "turbulent", presenting lots of local depletions, instead of the classical model or just a few gaps.

3.3 By Slope

This analysis was extremely impaired, since only one of the cases survived for both "One" and "Half". Still, some conclusions could be drawn comparing results between the slopes of the radial surface density profile (Figs. 3.8 and 3.9).

- Main: since 75% of the healthy simulations consisted of this group, is no surprise that the percentages for all properties (mass, semi-major axis, water mass fraction and eccentricity) are very similar to the general results. Worth noting, however, is that the average number of planets formed is larger than the one obtained with all simulations: 5.63;

- One: Percentages for water mass fraction and eccentricity are similar to general results. Planets tended to form much closer to the Sun (39% on the Inner than Earth group, against 31%, and just 15% on the Asteroid Belt, against 26%. Also no planet was formed on the Earth group region and 12% was formed on the Mars group region, though there are too few simulations to draw a relevant conclusion about that) and tend to be more massive as well: 15% on the Ceres group (against 26%), 9% on the Not Expected group (against 18%), 18% on the Earth group (against

8%) and there are 42% Super Earths (against 32%). The average number of planets formed is also smaller: 4.12;

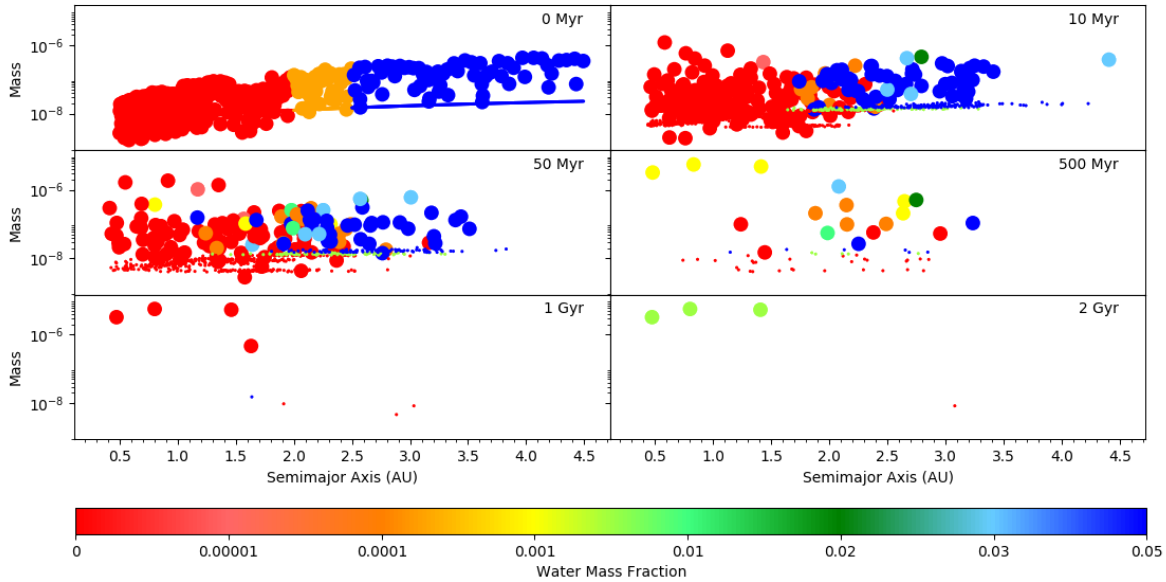

Figure 3.8: Snapchots for the masses as a function of semi-major axis of oemb3g3. Big circles represent embryos and small circles represent planetesimals. The final product is on the bottom right panel and the time of the snapchot is on the upper right corner of each panel. Note the depletions on the first panel and the water delivery process happening through time. Color coding represents the water-mass fraction of the body. Notice how there are less planets formed, compared to Fig. (3.7).

- Half: The tendency observed in "One" is also observed for this type. Whereas eccentricity and water mass fraction are similar to the general results, planets are even closer to the sun (37% Inner than Earth and 11% on the Asteroid Belt) and even more massive (11% Ceres, 18% Earths and 48% Super Earths). The average number of planets formed is smaller than "One": 3.38.

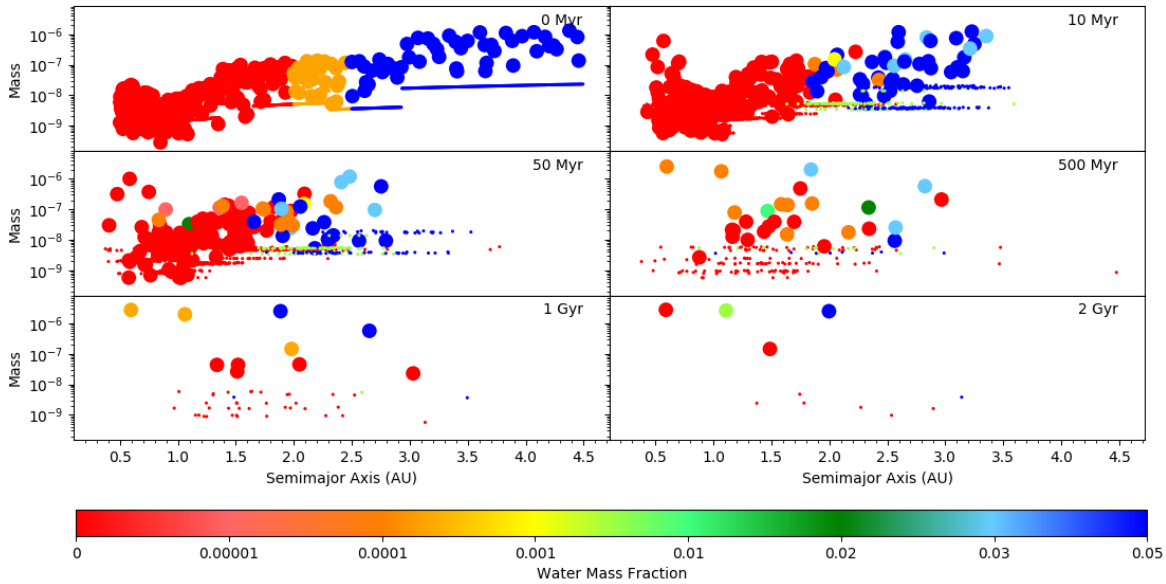

Figure 3.9: Snapchots for the masses as a function of semi-major axis of hemb2g5. Big circles represent embryos and small circles represent planetesimals. The final product is on the bottom right panel and the time of the snapchot is on the upper right corner of each panel. Note the depletions on the first panel and the water delivery process happening through time. Color coding represents the water-mass fraction of the body. Notice how the asteroid belt is "empty" and the inner planets are more massive. A Mars-like planet with 0.5 M_{Earth} is present at 1.49 AU.

In other words, smaller values of α tend to produce less planets, which are more massive and form closer to the Sun. This agrees with Raymond et al. (2005). More than that, the average number of embryos formed has a linear relation with the slope of the surface density profile (Fig. 3.10):

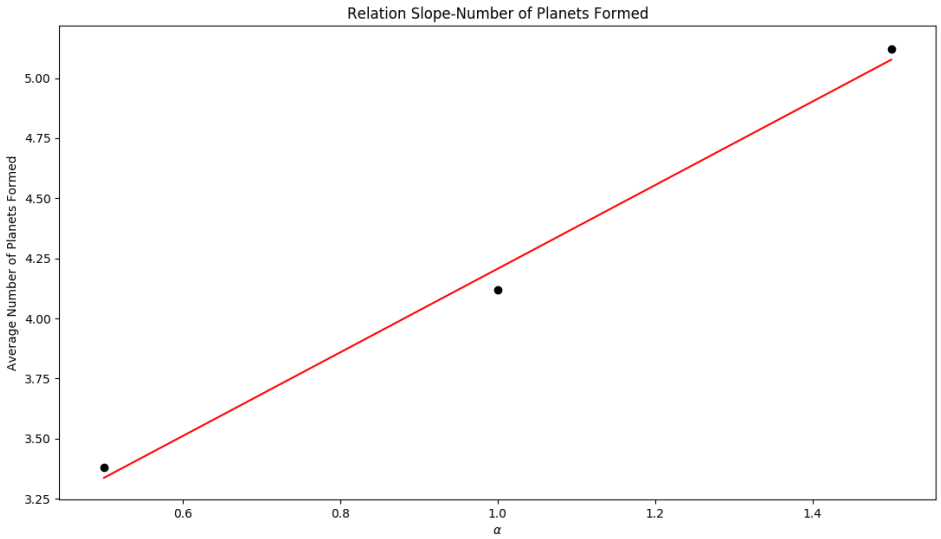

Figure 3.10: Average number of planets formed as a function of the slope. Linear fit is in red. Although there are few points (three), the relation is clear.

The adjusted line is:

$$\overline{P} = 1.74\,\alpha + 2.46$$

It has a p value of 0.05, which is relevant considering 95% of confidence level, and a Pearson Correlation Coefficient of 0.99.

Chapter 4

Conclusions

We ran a total of 128 simulations, with 8 distinct disk configurations and 8 distinct types of depletion. 64 of them "survived" and produced, on average, 3 to 7 planets. No Mars analog was formed; however, there were 16 Mars-like planets (8 more massive than Earth, 8 less massive), two of them deserving attention: one at 1.49 AU with 0.5 M_{Earth} and high eccentricity (0.462), and our "best result", a planet with 0.04 M_{Earth} at 1.59 AU, eccentricity of 0.135 and very wet (WMF of 0.05). We also produced 2 Earth Analogs and 18 Earth-like planets, of which only 3 are less massive than Earth.

58% of the 330 planets formed are either too light ("Super Asteroids", lighter than Mercury) or too massive (Super Earths), and 18% have masses that are not observed in any body of our inner Solar System (heavier than Mars, but lighter than Venus). All three terrestrial planets have similar chances of formation; massive planets (at least twice the mass of Earth) are rare. The majority of planets formed inside 1 AU or on the Asteroid Belt, and a significant amount (19%) formed on the "gap" observed between Mars and the core of the Asteroid Belt (1.6 AU to 2.5 AU). This might be explained by the effect of local depletions, which does not allow the embryos formed in those regions to throw away other bodies nearby. We also observe a bimodal distribution of water mass fraction (extremely dry or very wet), representing the populations of terrestrial planets that didn't accrete wet embryos scattered inside and asteroids that were "untouched" throughout the simulations. Only a small fraction of planets is eccentric (14% has $e > 0.2$), which is in accordance with what we observe in our inner Solar System.

The type of depletion changes the properties of the final ensemble, and special attention is needed for the disks with many gaps: their planets are more likely to form on Mars' and Earth's regions, and less likely to form on the Asteroid Belt - embryos further than 2 AU

have a greater chance to be scattered inwards (systems with few gaps produced contrary properties). They are also the only type that produced Earth analogs; the closest Mars analog and the only three Earth Like planets lighter than Earth were formed on a multi-gap disk as well. The slope of the radial surface density profile also impacts the systems: lower values of α produce less planets, which are heavier and closer to the Sun. Unlike the type of depletion, which does not influence on the average number of planets formed, we were able to derive a positive linear relationship between this property and α.

Even though we couldn't form a Mars analog, our results unmasked important relations between the depletions and slope of the disk and the inner Solar System formed. The variety of possible results is an amazing proof of the chaotic nature of planetary systems; it also suggests that exoplanetary systems found should have great diversity, which, observational bias discounted, holds true. Previous authors, like Izidoro et al. (2014) included *ad hoc* depletions and showed that a depleted disk was needed in order to solve the heavy Mars problem; our work extended theirs by introducing *random* depletions and indicating that not only a single gap depletion is needed, but probably *many* gaps. In other words, the nebular disk is rather inhomogeneous, presenting many local depletions. Still, more simulations need to be done to further validate these results: making a crude estimation, it would take about 1600 simulations, on average, to produce a system with Venus, Earth and Mars analogs. Our results also show that, because of this chaotic nature, it is extremely difficult to reproduce our Solar System exactly as it is observed today. Rather, our efforts should be focused on further exploring the depletion effects, to get a better understanding of how our nebular disk evolved. More slopes need to be simulated as well, to confirm (or reject) the linear relationship we found between them and the average number of planets formed. In essence, "planetary system cooking" is an arduous task, whilst exploring relations between initial configurations of the disk and system formed is, at least, palpable. Also, the inhomogeneity of the nebular disk implies a vastness of possibilites for planetary systems, once more showing how strikingly multifaceted the Universe is.

Bibliography

Boss A. P., Rapid formation of outer giant planets by disk instability, The Astrophysical Journal, 2003, vol. 599, p. 577

Brasser R., The formation of Mars: building blocks and accretion time scale, Space Science Reviews, 2013, vol. 174, p. 11

Chambers J. E., A hybrid symplectic integrator that permits close encounters between massive bodies, Monthly Notices of the Royal Astronomical Society, 1999, vol. 304, p. 793

Haghighipour N., The formation and dynamics of super-Earth planets, Annual Review of Earth and Planetary Sciences, 2013, vol. 41, p. 469

Haghighipour N., Winter O. C., Formation of terrestrial planets in disks with different surface density profiles, Celestial Mechanics and Dynamical Astronomy, 2016, vol. 124, p. 235

Hansen B. M., Formation of the terrestrial planets from a narrow annulus, The Astrophysical Journal, 2009, vol. 703, p. 1131

Izidoro A., de Souza Torres K., Winter O., Haghighipour N., A compound model for the origin of Earth's water, The Astrophysical Journal, 2013, vol. 767, p. 54

Izidoro A., Haghighipour N., Winter O., Tsuchida M., Terrestrial planet formation in a protoplanetary disk with a local mass depletion: A successful scenario for the formation of Mars, The Astrophysical Journal, 2014, vol. 782, p. 31

Jin L., Arnett W. D., Sui N., Wang X., An interpretation of the anomalously low mass of Mars, The Astrophysical Journal Letters, 2008, vol. 674, p. L105

Kokubo E., Genda H., Formation of terrestrial planets from protoplanets under a realistic accretion condition, The Astrophysical Journal Letters, 2010, vol. 714, p. L21

Kokubo E., Ida S., Oligarchic growth of protoplanets, Icarus, 1998, vol. 131, p. 171

Kokubo E., Ida S., Formation of protoplanets from planetesimals in the solar nebula, Icarus, 2000, vol. 143, p. 15

Lega E., Morbidelli A., Nesvornỳ D., Early dynamical instabilities in the giant planet systems, Monthly Notices of the Royal Astronomical Society, 2013, vol. 431, p. 3494

Mayer L., Quinn T., Wadsley J., Stadel J., Formation of giant planets by fragmentation of protoplanetary disks, Science, 2002, vol. 298, p. 1756

Morbidelli A., Chambers J., Lunine J., Petit J.-M., Robert F., Valsecchi G., Cyr K., Source regions and timescales for the delivery of water to the Earth, Meteoritics & Planetary Science, 2000, vol. 35, p. 1309

Morbidelli A., Lunine J. I., O'Brien D. P., Raymond S. N., Walsh K. J., Building terrestrial planets, Annual Review of Earth and Planetary Sciences, 2012, vol. 40, p. 251

Morishima R., Schmidt M. W., Stadel J., Moore B., Formation and accretion history of terrestrial planets from runaway growth through to late time: implications for orbital eccentricity, The Astrophysical Journal, 2008, vol. 685, p. 1247

O'Brien D. P., Morbidelli A., Levison H. F., Terrestrial planet formation with strong dynamical friction, Icarus, 2006, vol. 184, p. 39

Raymond S. N., O'Brien D. P., Morbidelli A., Kaib N. A., Building the terrestrial planets: Constrained accretion in the inner Solar System, Icarus, 2009, vol. 203, p. 644

Raymond S. N., Quinn T., Lunine J. I., Terrestrial planet formation in disks with varying surface density profiles, The Astrophysical Journal, 2005, vol. 632, p. 670

Thommes E., Nagasawa M., Lin D., Dynamical shake-up of planetary systems. II. N-body simulations of Solar System terrestrial planet formation induced by secular resonance sweeping, The Astrophysical Journal, 2008, vol. 676, p. 728

Walsh K. J., Morbidelli A., Raymond S. N., O'brien D. P., Mandell A. M., A low mass for Mars from Jupiter/'s early gas-driven migration, Nature, 2011, vol. 475, p. 206

Appendix

Appendix A

Extra Figures

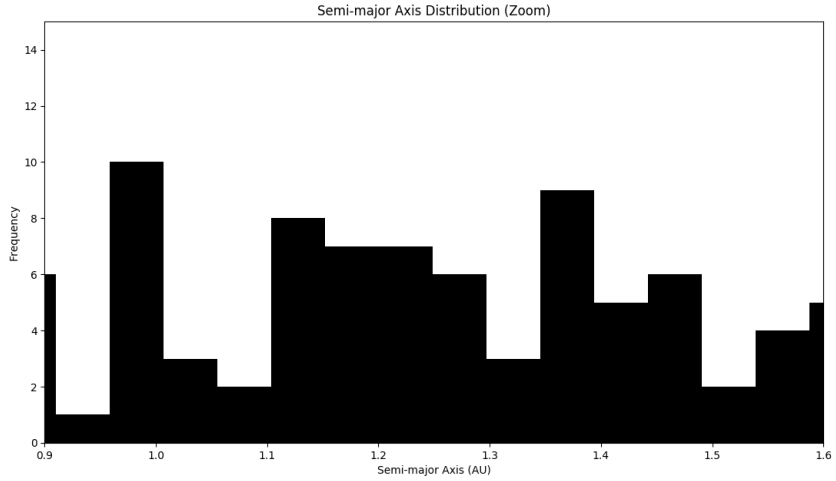

Figure A.1: Histogram of semi-major axis of all the planets formed by the 64 simulations with a zoom on the Earth/Mars analog region (0.9 AU to 1.6 AU).

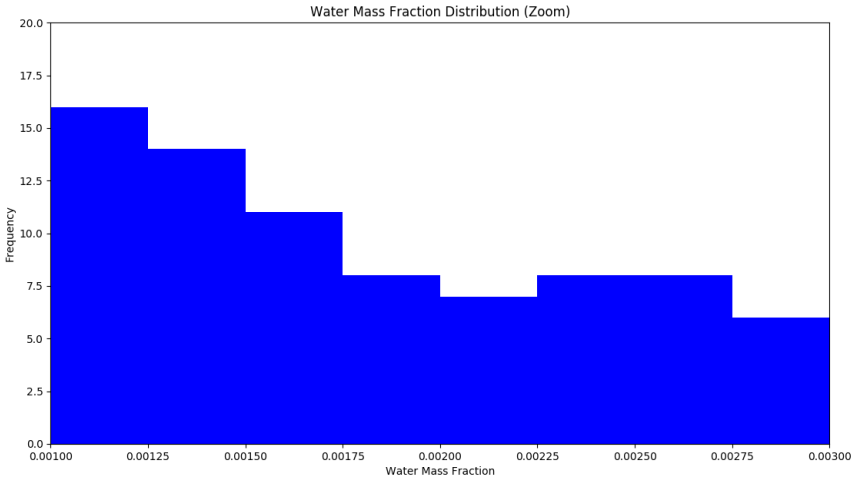

Figure A.2: Histogram of the water mass fraction of all the planets formed by the 64 simulations with a zoom on the "Earth WMF" region (0.001 to 0.003).